Primljen / Received: 17.6.2025.
Ispravljen / Corrected: 11.9.2025.
Prihvaćen / Accepted: 29.9.2025.
Dostupno online / Available online: 10.4.2026.

Preliminary investigation of vehicle weight estimation employing acoustic signals from bridge expansion joints

Authors:

Shichao Qian, MSc. CE
18155545324@163.com

Prof. **Xiaojuan Shu**, PhD. CE
254528003@qq.com
Corresponding author

Assoc.Prof. **Mingyan Shen**, PhD. CE
511272252@qq.com

Yili Luo,MSc. CE
154674841@qq.com

Haopeng Dang, MSc. CE
3026529583@qq.com

Hunan University of Science and Technology, China
Faculty of Civil Engineering

Research Paper

Shichao Qian, Xiaojuan Shu, Mingyan Shen, Yili Luo, Haopeng Dang

Preliminary investigation of vehicle weight estimation employing acoustic signals from bridge expansion joints

This study introduces a method for identifying vehicle load levels by analysing the characteristics of sound signals generated when vehicles pass over bridge expansion joints. The proposed approach is non-invasive and independent of lighting conditions, offering significant advantages. Experimental tests were initially conducted and effective impact sound signals were extracted by analysing the trend of the sound pressure amplitude following filtering, pre-emphasis, and signal detection processes. Typical characteristics of sound signals in the frequency, time, and time-frequency domains were extracted. The relationships between short-term energy, empirical mode decomposition (EMD) energy entropy, spectral centroid features, and vehicle weight were found to be significant for vehicle weight identification. Finally, a classifier based on the k-nearest neighbour (KNN) algorithm was employed for vehicle weight classification by analysing the identification results under varying vehicle speeds and feature parameters. The results indicated that the KNN classifier achieved high accuracy in vehicle weight identification: 90.8% at low speeds and 83.1% at high speeds. The confusion matrix revealed that misclassifications tended to predict vehicle weights in adjacent categories.

Key words:

vehicle weight recognition, expansion joint, acoustic signal, feature extraction, empirical mode decomposition (EMD)

Prethodno priopćenje

Shichao Qian, Xiaojuan Shu, Mingyan Shen, Yili Luo, Haopeng Dang

Preliminarno istraživanje procjene mase vozila na temelju zvučnih signala s prijelazne naprave mosta

Ovo istraživanje predstavlja metodu za određivanje razine opterećenja vozila analizom karakteristika zvučnih signala proizvedenih tijekom prelaska vozila preko prijelazne naprave mosta. Predloženi je pristup neinvazivan i neovisan o uvjetima osvjetljenja, zahvaljujući čemu ima znatne prednosti u primjeni. Na početku provedena su eksperimentalna ispitivanja, a potom su analizom linije trenda amplitude zvučnog tlaka izdvojeni relevantni udarni zvučni signali, pri čemu su prethodno primijenjeni procesi filtriranja, prednaglašavanja signala te detekcije signala. Iz zvučnih su zapisa izdvojene karakteristične značajke signala u frekvencijskoj, vremenskoj i vremensko-frekvencijskoj domeni. Utvrđeno je da odnosi između kratkotrajne energije, entropije energije dobivene metodom empirijskog razlaganja (EMD) te spektralnog centroida pokazuju znatnu povezanost s masom vozila, što omogućuje njihovu primjenu u identifikaciji mase vozila. Konačno, za klasifikaciju mase vozila primijenjen je klasifikator temeljen na algoritmu k-najbližih susjeda (KNN), pri čemu su analizirani rezultati identifikacije pri različitim brzinama vozila i parametrima značajki. Rezultati su pokazali da je KNN klasifikator, postigao visoku razinu točnosti u utvrđivanju mase vozila: 90,8 % pri malim brzinama i 83,1 % pri velikim brzinama. Matrica zabune pokazala je da su pogreške u razvrstavanju najčešće nastajale između susjednih kategorija masa vozila.

Ključne riječi:

prepoznavanje mase vozila, prijelazna naprava, zvučni signal, izdvajanje značajki, metoda empirijskog razlaganja (EMD)

1. Introduction

The assessment of the safety and durability of road and bridge infrastructures necessitates comprehensive vehicle load surveys and testing, which are crucial for maintaining structural integrity and longevity [1, 2]. A range of methodologies have been employed to collect pertinent data for vehicle information surveys and testing. These include:

- conventional static weighing scales
- dynamic weighing systems
- visual image recognition techniques
- acoustic and vibration signal recognition approaches.

Each method presents distinct advantages and limitations, particularly in terms of traffic flow and data accuracy.

Although the conventional static weighing scale method simple, it is limited by its inability to provide real-time data for passing vehicles, as vehicles must halt weighing. This requirement is impractical in high-traffic scenarios owing to the disruptions it causes [1]. By contrast, dynamic weighing systems offer a more fluid alternative, facilitating a continuous traffic flow. These systems can be categorised into two subtypes: pavement-based weigh-in-motion (PWIN) and bridge-based weigh-in-motion (BWIN). The PWIN utilises sensors embedded in the road surface and is susceptible to reduced longevity owing to the continuous pressure from vehicular traffic. Conversely, BWIN employs sensors integrated into a bridge structure, exploiting the dynamic responses induced by passing vehicles [3, 4]. By employing specific algorithms to deduce the stiffness distribution within the bridge, BWIN can accurately determine the vehicle axle loads, speed, and weight, providing a covert and non-invasive method of data collection.

Several studies have developed methods for identifying vehicle axle weights employing BWIM systems. For instance, Zhang et al. [5] used an iterative algorithm based on the Moses algorithm in conjunction with a measured influence-line algorithm to recognise vehicle axle weights in a BWIM system. Chen [6] developed a multivehicle BWIM system utilising long-gauge fibre Bragg grating sensors to identify vehicle speed, axle spacing, and weight. Kawakatsu et al. [7] proposed a single-sensor BWIM system employing deep neural networks to extract features such as lane information, vehicle speed, trajectories, and axle data using convolutional neural networks (CNNs). Deng et al. [8] proposed a multibridge dynamic weighing method employing CNNs.

Advancements in vehicle image recognition technology have been significant, particularly in achieving high accuracy in tasks such as reading licence plates, identifying vehicle types, and measuring speeds and sizes. However, although these technologies have reached a level of maturity, their limitations are becoming increasingly apparent, particularly in vehicle weight recognition. The primary challenge lies is that variations in vehicle weight are not readily discernible via appearance-based image features, even for identical vehicles or vehicle types. Consequently, research on vehicle-weight recognition employing visual imagery remains sparse. Several studies have explored the use of tire deformation in image recognition to estimate the vehicle weight, which requires high imaging precision. However, capturing high-definition images of tire deformation during rapid vehicle movements is challenging. Huan et al. [9] and Feng et al. [10] utilised this approach, highlighting the need for clear imaging of tire deformation. McKay et al. [11] proposed a method that employs a high-definition camera to capture the chassis torsion induced by engine torque, using these data to estimate vehicle weight. Similar to other methods that rely on structural deformation images, this approach encounters significant challenges. The primary disadvantages of using visual image recognition for vehicle weight include the stringent requirements for capturing the microscopic structural details and the interference from factors such as lighting, vehicle speed, and bridge vibration [12].

Acoustic signals, which are less intuitive than visual images, offer the distinct advantage of being unaffected by lighting conditions, making them a reliable choice for vehicle-parameter recognition [13-19]. The literature on vehicle type recognition employing sound signals is extensive, with early studies primarily focused on collecting road driving signals and employing single features of sound signals to classify vehicle types via shallow neural network models such as support vector machines (SVMs). For instance, Frederick et al. [16] utilised a fast Fourier transform (FFT) to extract peak frequency features from diesel and gasoline engine sound signals, employing an SVM for binary classification tasks with high accuracy. With the advancements in signal processing and artificial intelligence algorithms, the precision and scope of sound signal recognition have broadened significantly. Zhao Hongxu et al. [17] integrated a short-time Fourier transform (STFT), Mel-frequency cepstral coefficients (MFCC), and the fusion of STFT and MFCC features with an SVM for vehicle-type classification, demonstrating that combined features outperformed individual features in terms of recognition accuracy. Zhao et al. [19] employed principal component analysis (PCA) integrated with a backpropagation (BP) neural network (PCA-BP) to classify and identify the first two-order MFCC features of vehicle sound signals, effectively classifying vehicle speed and type. Chen [20] introduced an innovative approach by fusing three features of vehicle sound signals, namely MFCC, short-time energy features, and sound level contour features, and utilised a hybrid neural network that integrated a CNN with long short-term memory (LSTM) units for vehicle-type classification based on these new features.

Despite the proliferation of research on the use of acoustic signals for vehicle information recognition and achievement of high recognition rates in vehicle classification and speed

recognition, substantial reports on the utilisation of sound signals for vehicle weight recognition is notably absent [21]. When a vehicle is in motion, the sound signals collected from above the road are intricate, encompassing:

- mechanical sounds of the vehicle, such as those of the engine, transmission system, and collision sounds of vehicle components;
- frictional noise, including the friction sounds between the wheels and ground and between the vehicle body and air; and
- environmental white noise [22-24].

Frictional sound is particularly sensitive to vehicle speed and forms the basis for speed recognition [22, 23]. Distinct vehicle models exhibit characteristic acoustic signatures related to their engines and transmission systems, which are essential for vehicle recognition [14]. Theoretically, when the weight of a vehicle changes under constant conditions, alterations in the mechanical and frictional sounds between the wheels and road surface should be more pronounced than changes in the vehicle body shape typically observed in images. Therefore, recognising the vehicle weight based on sound signals is plausible. If a consistent "defect" is established during driving, such as speed bumps or expansion joints, the variations in sound owing to changes in weight become more apparent [25, 26]. Ravshanovich et al. [25] conducted noise tests of vehicles passing through modular expansion joints and identified a primary frequency of 500 to 800 Hz from the noise generated from the top of the expansion joint. This frequency is attributed to resonance noise caused by changes in air pressure in the cavity of the rubber sealing strip between modular beams influenced by vehicle movement. The primary frequency of the noise generated from the bottom of the expansion joint is lower than 200 Hz, resulting from the vibration of the steel beam of the modulus expansion joint. Ghimire et al. [26] investigated the noise mechanism of modular expansion joints employing finite vibration elements and acoustic boundary element methods and observed the primary vibration frequency component of the structure in the noise analysis of the expansion joint cavity. They suggested a potential interaction between the structural mode of the expansion joints and the acoustic mode of the cavity, implying that the vibration signal caused by the structural stress can be reflected in the acoustic signal. Single-slot U-shaped expansion joints, widely used in approach bridges of large bridges and in the structures of medium and small bridges, serve as an ideal "impact sounder" when vehicles are travelling [27]. Leveraging on this concept, this study investigated the recognition of different vehicle weight levels based on the acoustic signal characteristics of tripping an expansion joint.

The process by which vehicles pass through expansion joints can be analogous to the relative sliding process observed in mechanical transmission systems, such as the interaction between gears, rolling elements of bearings, and the inner and outer rings. When defects such as cracks are present on the gear plate or bearing ring, the sound emitted during sliding at the defect site differs significantly from that under normal conditions. This principle forms the foundation of acoustic signal-based mechanical fault diagnosis [28-31]. The challenge in diagnostics lies in the precise discrimination of defect types and severity (e.g. crack width) in complex background noise. The enhancement of the signal-to-noise ratio is a crucial aspect of signal detection. Lu et al. [32] employed the threshold double-threshold method to detect pulse sound signals caused by impact defects, thereby improving the accuracy of endpoint detection. Hou et al. [33] introduced a sparse-based multipoint optimal minimum entropy deconvolution adjustment (MOMEDA) method, which was applied to enhance and diagnose bearing fault characteristics employing sound signals. Signal fusion and weighting techniques can further amplify the signal weights of fault sounds. For instance, Li et al. [34] proposed a novel method that integrates multimodal sound and vibration sensor signals to extract the fault characteristics of vibration and sound signals, thereby addressing the issue of early fault characteristics being masked by strong background noise. Di Pei et al. [35] utilised autocorrelation calculations and empirical mode decomposition (EMD) to suppress noise. Furthermore, they reconstructed and strengthened fault information employing the cross-correlation coefficient kurtosis index; subsequently, they extracted fault feature frequency employing Teager energy operator analysis to achieve state monitoring of early weak fault information in bearings. Shi et al. [36] proposed a two-stage sound and vibration signal fusion algorithm employing grey B-type correlation weighting, EMD, and kurtosis superposition to enhance the signal-to-noise ratio of fault features. Different sound signal characteristics have varying indicative significances for fault signals. Yang et al. [37] proposed a feature fusion method employing entropy-weighted interference attribute projection (EWNAP) and orthogonal locality-preserving projection (OLPP) to obtain fault-sensitive features for identifying rolling-bearing faults via backpropagation (BP) neural networks. Mian et al. [38] emulated human acoustic perception using a HATS to obtain sound signals, provided a bearing fault diagnosis based on sound-quality features, and described various sound-quality features under different fault conditions. In terms of intelligent classification algorithms, artificial intelligence algorithms such as KNN, CNN, RNN, and LSTM have been applied to fault diagnosis and vehicle identification [39-46]. Fuzzy dispersion entropy (FuzzDE) is a recently proposed nonlinear dynamic indicator that combines the strengths of both dispersion entropy (DE) and fuzzy entropy (FuzzEn) to detect dynamic changes in a time series. Li et al. [47] introduced fractional order calculation based on FuzzDE, proposed FuzzDEα, and employed it as a feature for signal analysis and fault diagnosis

of bearings. Coded permutation entropy has been proposed to enhance noise immunity via quadratic partitioning on the basis of permutation entropy. Li et al. [48] applied the concept of quadratic partitioning to DE, leveraging the ability of DE to effectively measure amplitude information, and proposed coded DE (CDE), which increases the number of patterns and improves divisibility by further coding the dispersion patterns in DE.

In mechanical failure diagnosis, expansion joints can be likened to defects with a deterministic degree. However, unlike the rotational force applied in conventional diagnostics, changes in sound signals are utilised to discern variations in the applied force. In this study, the acoustic responses of heavy-duty vehicles passing through a U-shaped expansion joint on a bridge at different speeds and weights were used to capture "jumping" sound signals. Subsequently, the sensitivity of several sound signal characteristics to vehicle weight was examined. Based on the sensitivity analysis, valuable sound signal feature parameters for weight identification were proposed. Employing the k-nearest neighbour (KNN) algorithm, a preliminary study classified and identified the weight level of a specific type of heavy-duty vehicle. The remainder of this paper is organised as follows: Section 2 details the experiment and data collection process, Section 3 outlines the pre-processing of acoustic signals, Section 4 describes the extraction of signal features and their statistical rules, Section 5 presents the results of the weight classification analysis using the KNN algorithm, and Section 6 concludes the study.

2. Assessment for collecting impact sound signals of a heavy-duty truck traversing an expansion joint

2.1. The experimental site and the collection scheme

The experimental site was strategically selected in the midsection of a straight, orthogonal bridge with a length exceeding 200 m and characterised by a low traffic volume. This particular section comprises an expansion joint perpendicular to the bridge axis; specifically, a single U-shaped steel expansion joint with a width of 60 mm. The surrounding area, within a 500-meter radius, is relatively spacious and free from tall buildings or dense vegetation, resulting in minimal environmental noise and the absence of echo effects. During the experiment, acoustic signals generated by heavy-duty vehicles of varying weights and speeds were collected, as they traversed the road section, including the expansion joint. The microphone for the experiment was positioned along the sidewalk, 8.8 meters away from the centreline of the vehicular traffic. A diagrammatic representation of the site layout is shown in Figure 1. The sound signal acquisition commenced when the vehicle reached Section A and terminated upon reaching Section B. The distance between Sections A and B along the traffic flow was 20 m, and the microphone was located midway on the corresponding sidewalk. An INV9206 sound pressure sensor was used as the microphone, in conjunction with a cloud-intelligent data acquisition device, INV3062T. The system was capable of measuring sound intensities up to 146 dB and supports a maximum sampling frequency of 51.2 kHz. Images of the experimental site and equipment are displayed in Figure 1 and a schematic of the testing protocol is delineated in Figure 2.

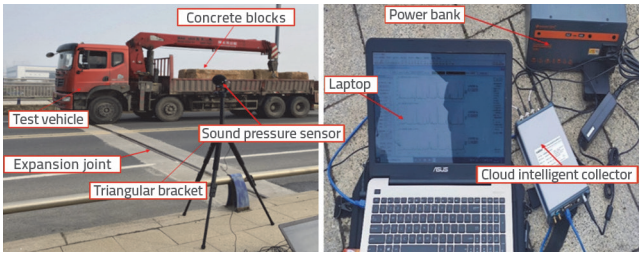

Figure 1. Experiment site and experimental instruments

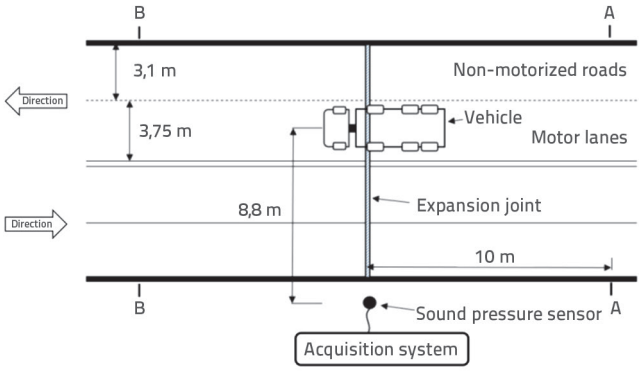

Figure 2. Layout of the testing scheme

2.2. Design of the jumping conditions of the vehicle crossing the expansion joint

The experimental vehicle used in this study was a Dongfeng Huashen-brand four-axle heavy-duty crane with a net weight of 18.4 tons. The concrete blocks were stacked to vary the total weight of the vehicle. Each concrete block had a mass of 3.19 tons, and the maximum weight conFigure uration reached 34.4 tons, which was achieved by adding five concrete blocks to the vehicle, thereby attaining six weight levels. The vehicle was subsequently driven over the expansion joint at two distinct speeds: 30 km/h and 50 km/h. The acoustic data of the tripping sound signals were collected as the vehicle traversed from section A to section B across the expansion joint. A summary of the driving parameters of the experimental vehicles is presented in Table 1.

Table 1. Driving parameters of the experimental vehicle

Parameter items	Parameter value	Load level	Vehicle weight [ton]	Speed
Overall dimensions [cm]	1200 × 255 × 399	1	18.4	
Lateral track width [cm]	185	2	21.5	
Front-mid wheelbase [cm]	215	3	24.8	30 km/h
Mid-rear wheelbase [cm]	440	4	28.0	50 km/h
Rear-rear wheelbase [cm]	135	5	31.1	
Tire type	Steel wire tire 11.00R20	6	34.4	

3. Acoustic signal pre-processing

The acoustic signals collected from a vehicle traversing the expansion joint in an outdoor environment are inherently complex and comprise multiple components. To enhance the signal-to-noise ratio, reduce the computational burden of data analysis, and improve the efficiency of the analysis, it is imperative to conduct appropriate preprocessing of acoustic signals. The acoustic signal preprocessing is illustrated in Figure 3. Initially, the raw signals captured by the microphone were subjected to low-pass filtering to mitigate the effects of wind pressure. Subsequently, the non-impacting segments at the extremities of the initial signal were truncated, thereby reducing the data volume and enhancing the analysis efficiency. The third step involved downsampling to eliminate the ultrahigh-frequency (UHF) noise. The fourth step applied pre-emphasis to the signal. Following the third and fourth steps, the signal-to-noise ratio was further enhanced. Finally, the signal was segmented into frames and windowed, thereby partitioning and stabilising the nonstationary signal. Sections 3.1 and 3.4 detail the methodologies employed for each step of the preprocessing sequence.

3.1. Signal filtering and down-sampling

The acoustic signals captured from above the road surface during the tripping process of the expansion joint encompass a range of components, including automotive mechanical noise (predominantly noise from engine and mechanical transmission), wind noise, road noise (resulting from friction between the ground and wheels), and short-term impact noise emanating from the expansion joint owing to tire impact. Wind noise is considered velocity-dependent and is not significantly influenced by vehicle weight, whereas other noise components may exhibit weight-dependent characteristics. Based on the initial signal analysis and a review of the literature on the characteristics of driving acoustic signals, the primary frequency range of driving sound signals collected at the expansion joints on bridge roads was found to be within 8 kHz [17, 19]. In accordance with the Nyquist sampling theorem, the down-sampling frequency was set to twice the frequency of interest (16 kHz). A high-pass filter with a lower-limit frequency of 20 Hz was applied to eliminate low-frequency noise, such as that caused by wind pressure. Figures 4 illustrates the signals before and after filtering.

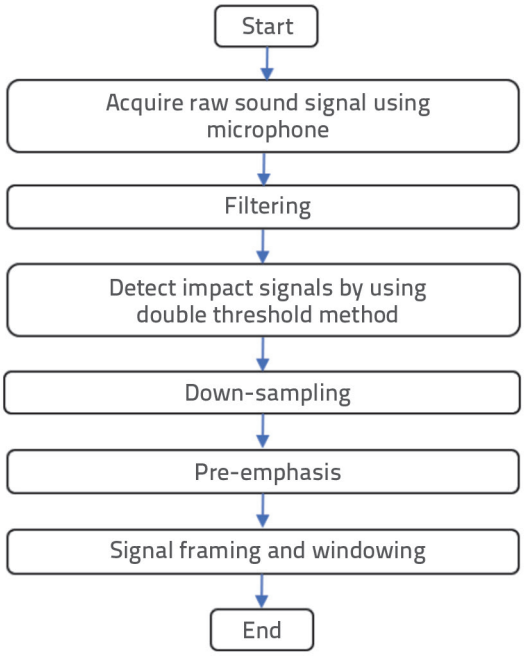

Figure 3. Process of signal pre-processing

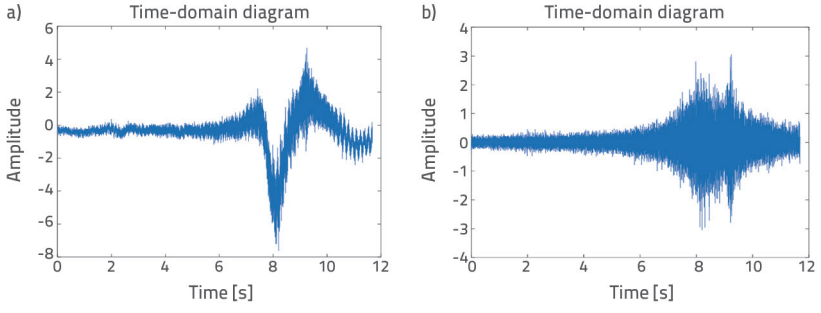

Figure 4. Signal filtering: a) Initial signal; b) Filtered signal

3.2. Detection and interception of impact signals based on the trend line of sound pressure amplitude envelope

Each audio signal was recorded during the vehicle's traversal from section A to section B, capturing both the acoustic signal generated when the vehicle travels over the expansion joint and the sound produced while driving on ordinary road sections. The signal values associated with the non-impact process of driving on ordinary roads were deemed insignificant; therefore, these were truncated to reduce the length of the signal. Consequently, detecting and segmenting audio signals is essential for eliminating redundant signals and enhancing the analysis efficiency. This study employed a method based on the trend line of the sound pressure amplitude envelope to segment the impacting sound signal [42]. The sound pressure envelope was derived using the root mean square energy (RMS) method, which increased the robustness of the envelope to outliers. This was achieved by calculating the sum of the squares of the sound pressure values within a window, dividing it by the frame length, and using the square root to yield the envelope value for that frame. The mathematical definition of this energy calculation is given in Equation 1:

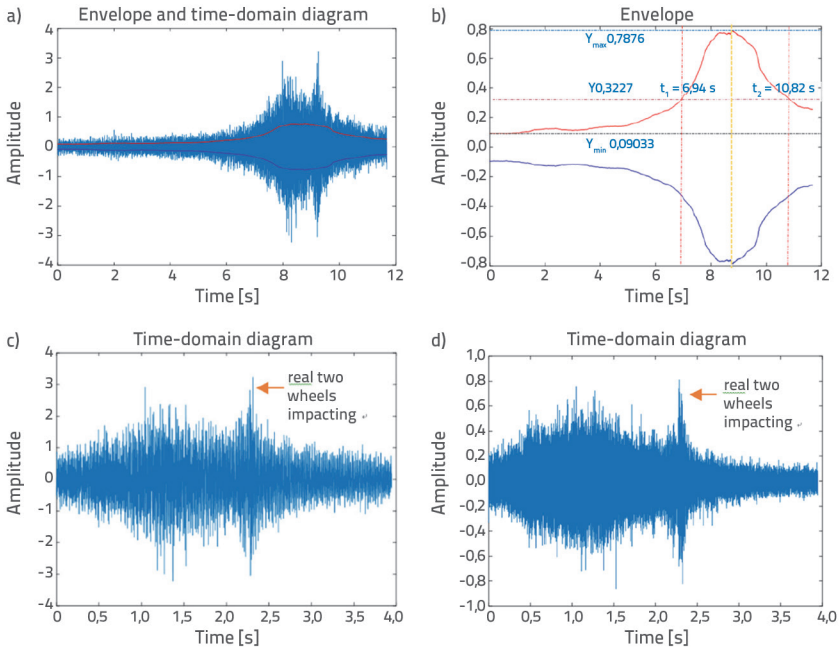

Figure 5. Process of signal pre-processing: a) Envelope of sound pressure amplitude; b) Threshold detection and interception; c) Intercepted signal; d) Signal after pre-emphasis

$$RMS_t = \sqrt{\frac{1}{K}\sum_{k=tK}^{(t+1)K-1} x(k)^2} \quad (1)$$

In Equation (1), t denotes the number of windows, K represents the number of samples within each window, and $x(k)$ is the sample function within the window, which corresponds to the sound pressure amplitude function. For this study, KK was set to 50,000. The calculated sound pressure envelope is shown in Figure 5a.

As illustrated in Figure 5, the process involves searching for the peak value of the trend line after obtaining the envelope trend line, as shown in Figure 5a a. Forward and backward searches were conducted using peak values. After identifying a certain threshold, the signal segments preceding and succeeding the two limiting lines are excised. The search threshold established in this article is defined by Equation (2),

$$RMS_l = \gamma_{min} + (\gamma_{max} - \gamma_{min})/3 \quad (2)$$

where γ_{min} and γ_{max} are the minimum and maximum values of the upper envelope trend line, respectively, as demonstrated in Figure 5.b. In Figure 5.b, the yellow vertical line indicates the peak position of the trend line, and the two red vertical lines indicate the start and end points of the impact signal. The signal length after detection and segmentation is shown in Figure 5c.

3.3 Signal pre-emphasis

The detected signal segment still comprised a substantial number of non-impulse noise signals. Impulse signals, which are characteristic of instantaneous events, are typically represented as high-frequency signals. Applying a pre-emphasis to the signal can mitigate the attenuation rate of these high-frequency components without significantly affecting the noise. This process effectively enhanced the signal-to-noise ratio, thereby highlighting the features of the acoustic signal resulting from the instantaneous impact of the vehicle traversing the expansion joint. The pre-emphasis technique was implemented using a transfer function, as shown in Equation (3).

$$H_x = 1 - \alpha x^{-1} \quad (3)$$

where x represents the amplitude of the original signal, and α is the pre-emphasis coefficient, which was taken as 0.97 in this study. A waveform comparison before and after pre-emphasis is shown in Figure 5.c and Figure 5.d, which amplifies the tripping impact signal.

The acquired sound signal is categorised as a non-stationary signal, necessitating the introduction of the "short-time" concept to segment the signal into multiple frames that can be approximated as stationary models. Assuming that a signal remains approximately stationary within a duration of 10 to 30

ms is typical in signal processing. In this study, the frame length was set to 30 ms with a frame shift equivalent to half the frame length. This approach facilitates a more manageable analysis by treating each frame as a short stationary segment.

The application of signal windowing techniques, such as the Hamming window selected for this study, smoothens the overlapping parts of adjacent frames and mitigates spectrum leakage, which is crucial for accurate frequency domain analysis [22, 43]. The use of a Hamming window is particularly beneficial owing to its ability to reduce discontinuities at the edges of frames, thereby providing a more gradual transition and a more stable spectral estimate.

3.4. Empirical modal decomposition (EMD)

EMD is an integral part of the Hilbert-Huang transform (HHT). This signal decomposition method is suitable for the analysis of nonstationary signals and is adaptable without the need for parameter input. EMD can adaptively decompose a signal from high to low frequencies into several intrinsic mode functions (IMFs) and residual terms. These IMFs represent the components of the acoustic signal across a range of frequency bands. The steps for the EMD calculation are illustrated in Figure 6.

The output criteria for an IMF are that the mean of the upper and lower envelopes at any given point equals zero, and that the difference between the number of extremum points and the number of zero crossings is not greater than one. The extraction of the IMFs was conducted in accordance with the EMD calculation steps, and the final signal component that did not meet the IMF criteria was considered the residual term. Six IMFs were successfully extracted.

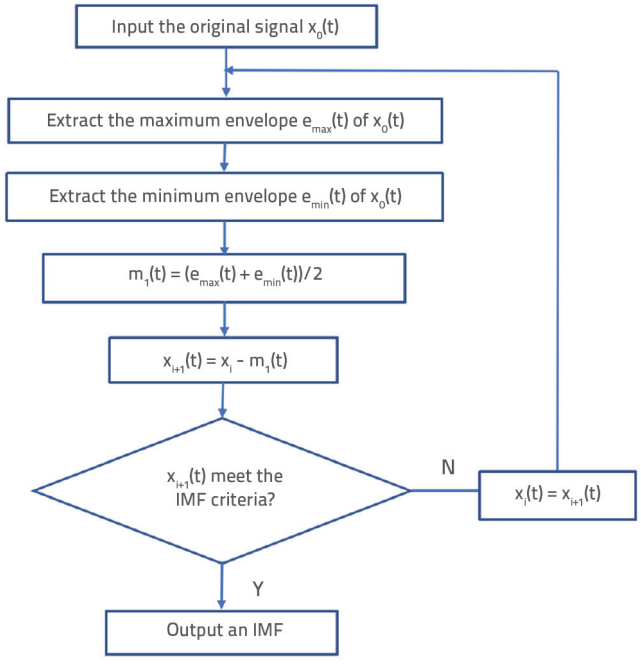

Figure 6. EMD calculation steps

4. Statistical analysis of correlation between sound signal characteristics and vehicle weight

4.1. Feature extraction

In this study, numerous features from the vehicle tripping acoustic signal were extracted for analysis, comprising time-domain features such as short-time zero-crossing rate and short-time energy, and frequency-domain features such as spectral centroid, spectral spread, spectral entropy, spectral flux, and the proportion of EMD energy entropy and IMF energy [31]. After a comprehensive comparison, the analysis revealed that the features exhibiting relative sensitivity to vehicle weight recognition and consistent discriminative patterns included short-term energy, spectral centroid, spectral entropy, and EMD energy entropy.

The short-term energy, E_n, denotes the energy contained within each frame of the signal; therefore, the analysis focused on the framed and windowed signals. Mathematically, it is expressed as the sum of the squares of the acoustic signal amplitudes in each frame, as depicted in Equation (4).

$$E_n(m) = \sum_{m=0}^{N-1} x_n^2(m) \tag{4}$$

Where $x_n(m$ is the mth sampling point of the n -th frame signal and Nrepresents the frame length.

The spectral centroid S.C. is the first-order central moment of the spectrum, which is indicative of the frequency-centre content of the gravitational acoustic signal. The calculation is as follows:

$$SC = \frac{\sum_{n=0}^{N-1} f(n)E(n)}{\sum_{n=0}^{N-1} E(n)} = \sum_{n=0}^{N-1} f(n)P(E(n)) \tag{5}$$

where $E(n)$ is the spectral energy of the corresponding frequency after the STFT of the discrete time-domain signal, N is the signal length, $P(E(n))$ represents the proportion of the energy at each point to the total energy, and $f(n)$ is the frequency of the transformed signal at a certain point.

The entropy was used to measure the degree of dispersion and uncertainty within the signals. EMD energy entropy indicates the degree of energy distribution disorder in different frequency bands and is commonly used in fault diagnosis [42-44]. Its mathematical expression is presented in Equation (6).

$$H_E = -\sum_{j=1}^{m} p_j \log p_j$$
$$p_j = \frac{E_j}{\sum_{j=1}^{m} E_j} \tag{6}$$

Here E is the total energy, p_j is the energy proportion of the j-th IMF, and H_E is the energy entropy of EMD. The IMF extraction steps are presented in [14].

The mathematical expression for spectral entropy is similar to that in equation (5). The spectral entropy can be derived by changing the calculation of p_i to the proportion of the spectral amplitude of the jth IMF.

Furthermore, statistical parameters were extracted from the time- and frequency-domain features, including five statistical parameters (mean, median, maximum, standard deviation, and kurtosis [29, 30, 44], to analyse and assess the sensitivity of these features to vehicle weight.

4.2. Statistical characteristics of the four features

Following the preprocessing of vehicle-tripping sound signals at multiple load levels and speeds, short-term energy-parameterised features were extracted and normalised to standardise the feature values within the range of 0 to 1 [45]. The parametric statistical analysis results for the short-term energy characteristics at driving speeds of 30 and 50 km/h are depicted in Figure 7.

The analysis in Figure 7a reveals that the characteristic parameters do not exhibit a clear pattern with increasing load levels; however, a general upward trend is observed in the overall values of each parameter. At a speed of 50 km/h, the mean, median, maximum, and standard deviation parameters of the short-term energy of the sound signal increased progressively from load levels 1 to 5; however, they exhibited a decrease at load level 6. The kurtosis index shows a significant decrease only when the load level increases from the fourth to the fifth level, whereas under other operating conditions, it increases as the load level increases.

Preliminary spectral analysis of the tripping sound signal indicated that the proportion of high-frequency energy in the spectrum increased with the vehicle weight, as illustrated in Figure 8. This suggests a correlation between the high-frequency components of the impacting sound signal and vehicle weight. Consequently, further exploration of frequency-domain features that can be utilised for vehicle weight recognition is warranted.

The statistical outcomes of the spectral centroid characteristics are presented in Figure 9. At the low speed of 30 km/h, the spectral centroid exhibited minimal variation with increasing vehicle weight. However, at a higher speed of 50 km/h, a significant upward trend was observed in both the mean and median values, whereas the other indicators did not follow a consistent pattern. The correlation between the spectral centroid and vehicle weight was relatively low at lower speeds; however, it became more pronounced at higher speeds.

The statistical results of the spectral entropy calculations are displayed in Figure 10. As shown in Figure 10, the relationship between the spectral entropy and vehicle weight aligns with that observed for the spectral centroid. With the exception of the peak and maximum values, the other indicators demonstrated an increasing trend in correlation with vehicle weight at the higher speed of 50 km/h.

Figure 11 illustrates the EMD energy entropy feature, energy proportion of the IMF components, and EMD energy entropy extracted from the pre-processed vehicle "jumping" sound signals at different load levels and speeds of 30 and 50 km/h.

Figure 11 shows that the proportion of the IMF energy for vehicles of varying weights decreased as the load level increased at a speed of 30 km/h. This trend suggests that the frequency content of the acoustic signal shifts towards higher

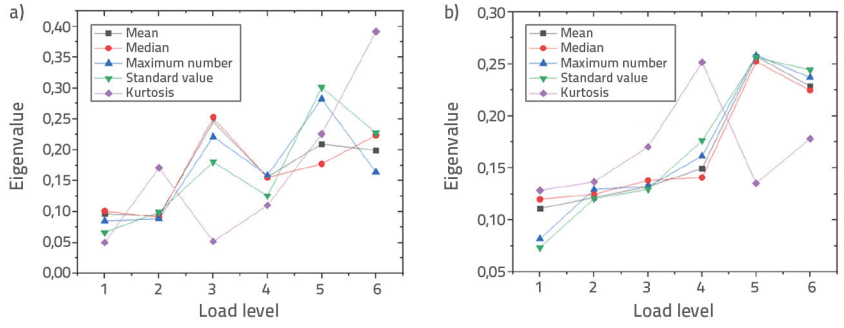

Figure 7. Relationship between vehicle weight and short-term energy parameters: a) 30 km/h b) 50 km/h

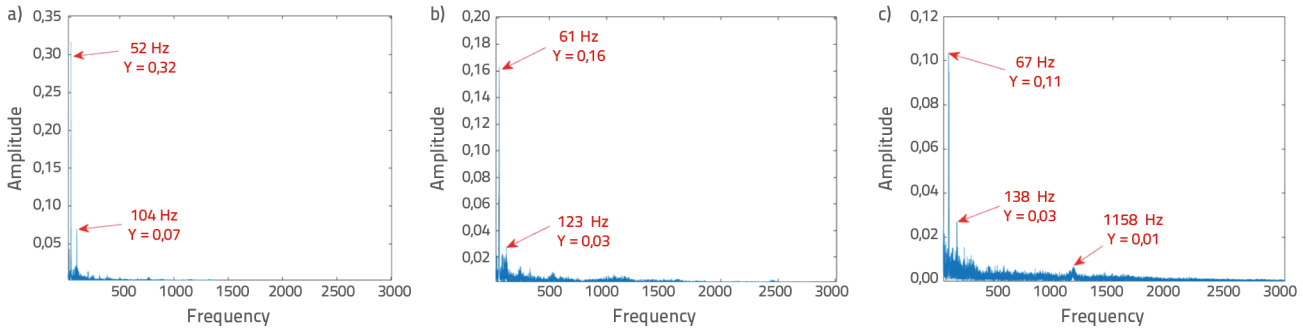

Figure 8. Spectrum distribution of different vehicle weights: a) load level 1; b) load level 3; c) load level 5

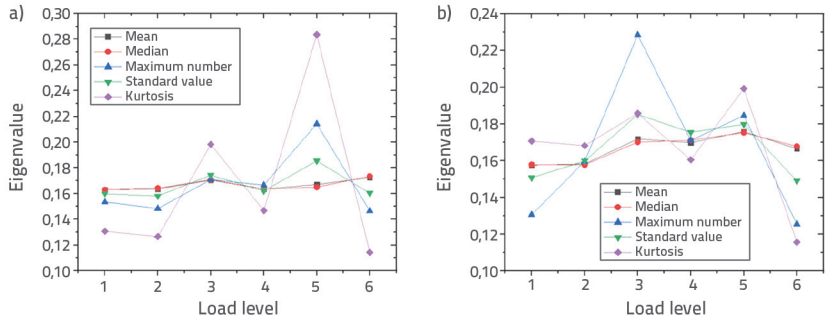

Figure 9. Relationship between vehicle weight and spectral centroid parameters: a) 30 km/h; b) 50 km/h

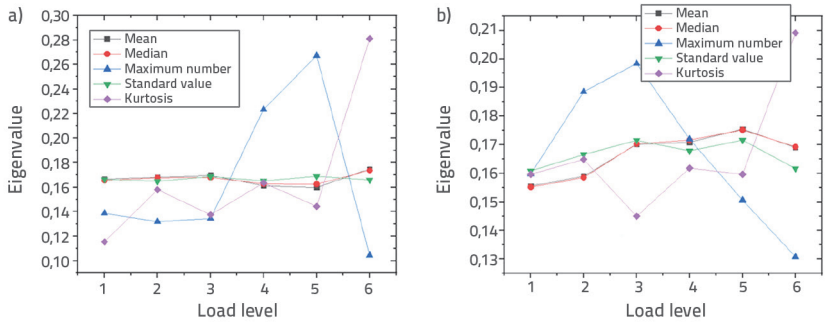

Figure 10. Relationship between vehicle weight and spectral entropy parameters: a) 30 km/h; b) 50 km/h

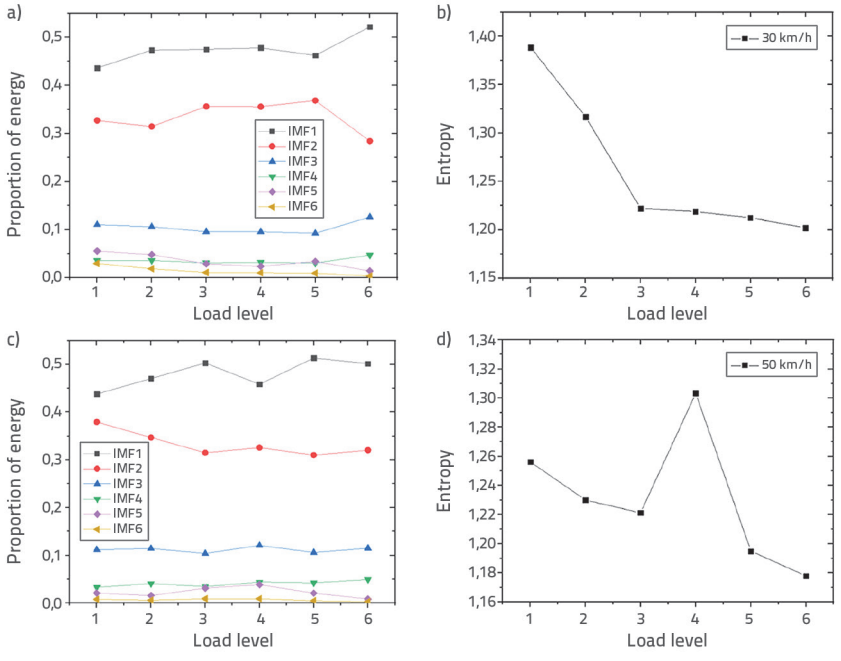

Figure 11. Relationship between vehicle weight and EMD energy entropy parameters: a) Proportion of energy at 30 km/h; b) Entropy at 30 km/h; c) Proportion of energy at 50 km/h; d) Entropy at 50 km/h

frequencies at this speed, concurrent with a reduction in energy within the low-frequency band. In addition, the EMD energy entropy decreases as the load level increases, and the entropy values for the initial two load levels exhibit significant changes. At 50 km/h, no distinct pattern was observed in the IMF energy proportions across the different vehicle weights. The entropy value increased when the load level reached 4, whereas in other instances, it decreased as the load level increased. A strong correlation was identified between the EMD energy entropy feature and vehicle weight when analysing the tripping signals.

5. Comparison of vehicle weight classification results based on KNN and different feature sets

5.1. Development of acoustic signal feature sets

Section 4 explored the qualitative relationship between multiple time and frequency spectral features and vehicle weight; however, no single feature can establish a simple quantitative calculation model with vehicle weight. Therefore, the use of artificial intelligence algorithms is necessary to obtain intrinsic quantitative connections. Owing to the limitations of research funding, the number of samples from real bridge tests was relatively limited; therefore, this study only conducted preliminary quantitative analysis and load level identification.

The feature sets utilised for vehicle weight recognition from acoustic signals comprised four categories: short-term energy, spectral centroid, spectral entropy, and EMD energy entropy. The data for each of these features, namely short-term energy, spectral centroid, and spectral entropy, were structured as a 1×5 feature vector encompassing the mean, median, maximum, standard deviation, and kurtosis. By contrast, the EMD energy entropy feature data were structured as a 1×7 feature vector, which included the entropy and proportional energy contributions of the first six IMF components.

Post-preprocessing, the feature database of the acoustic signal contained 187 samples, with 91 samples corresponding to the impact sound signals at 30 km/h and 96 samples corresponding to those at 50 km/h. The detailed compositions of the samples are presented in Table 2.

Table 2. Driving parameters of the experimental vehicle

Vehicle speed	Total num. of samples	Load levels					
			2	3	4	5	6
30 km/h	91	12	18	15	16	15	15
50 km/h	96	15	15	18	15	18	15

5.2. K-nearest neighbour algorithm

The sample size of the present study was modest. Deep neural network models such as CNNs, typically require a substantial number of samples for effective classification and recognition [29, 41]. Consequently, this study opted for the K-nearest neighbour (KNN) algorithm, a traditional shallow machine learning algorithm that is suitable for small-sample recognition tasks [40]. The KNN algorithm offers several advantages over other methods such as SVM and linear regression. These include the capacity to seamlessly integrate new data and the significantly faster computational speed. Within a predefined training set, the KNN algorithm identifies the k samples closest to the test sample and employs the k-nearest samples to determine the classification categories. The classification process is illustrated in Figure 12.

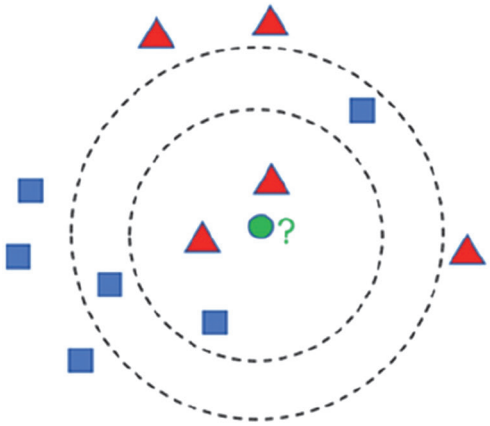

Figure 12. KNN classification principle

As shown in Figure 12, when k=3, the test sample is surrounded by two red triangles and one blue square, with red triangles being the majority. Consequently, the green circle was classified as a red triangle. When k=5, the test sample is encircled by two red triangles and three blue squares, with the blue squares representing the majority. Therefore, the green circles are classified as blue squares. To determine the most similar sample, it is imperative to calculate the similarity, or more precisely, the distance between the test and training points.

In summary, the KNN algorithm is primarily influenced by three factors:

- The distance metric, which quantifies the similarity between the test and training points. This study employs the Euclidean distance as the metric for measuring distance [43]
- classification decision rule, which typically follows the principle of majority voting and assigns the test point to the category with the highest proportion among its nearest neighbours
- selection of the kk value, which determines the number of nearest training points to be considered for classification based on their proximity and the classification decision rule.

Through validation, the KNN model in this study achieved optimal classification performance when k = 3. The n-fold cross-validation method was used to prevent model overfitting. This method partitions a dataset into five mutually exclusive subsets, using one subset as the test set and the remaining subsets as the training set. After five iterations of training and testing, the average of the five test results was used as the final outcome.

5.3. Analysis of Vehicle Weight Recognition Results

The KNN algorithm was employed to classify the vehicle weight based on the four types of feature parameters derived from the vehicle impacting the sound signal at the expansion joint. The classification results are listed in Table 3.

As shown in Table 3, the impacting sound signal at a lower speed of 30 km/h exhibited superior performance in vehicle weight classification when utilising the short-term energy and EMD energy entropy features. Specifically, the classification accuracy based on EMD energy entropy was 90.8 %, whereas the accuracy based on short-term energy reached 81.4 %. For the impacting sound signal at a higher speed of 50 km/h, the spectral centroid, spectral entropy, and EMD energy entropy features demonstrated improved performance in vehicle weight classification, with recognition accuracies exceeding 70 %.

When incorporating only the accuracy recognition rate, the aforementioned features may not significantly influence the recognition of vehicle weight levels. However, this experiment set a high-precision requirement for vehicle weight recognition. The weight difference between adjacent classes was 3.19 tons, which was only 0.173 times the net weight of the vehicle. Therefore, even if the vehicle weight is classified into an adjacent category, this indicates a certain level of accuracy in vehicle weight recognition [45, 46]. Figures 13 and 14 show the confusion matrices for vehicle weight classification based on short-term energy, spectral centroid, spectral entropy, and EMD energy entropy characteristics, respectively.

Table 3. Vehicle weight classification results based on acoustic characteristics

Speed	Short-term energy	Spectral centroid	Spectral entropy	EMD energy entropy
30 km/h	81.4 %	45.2 %	58.2 %	90.8 %
50 km/h	60.2 %	83.1 %	75.4 %	74.3 %

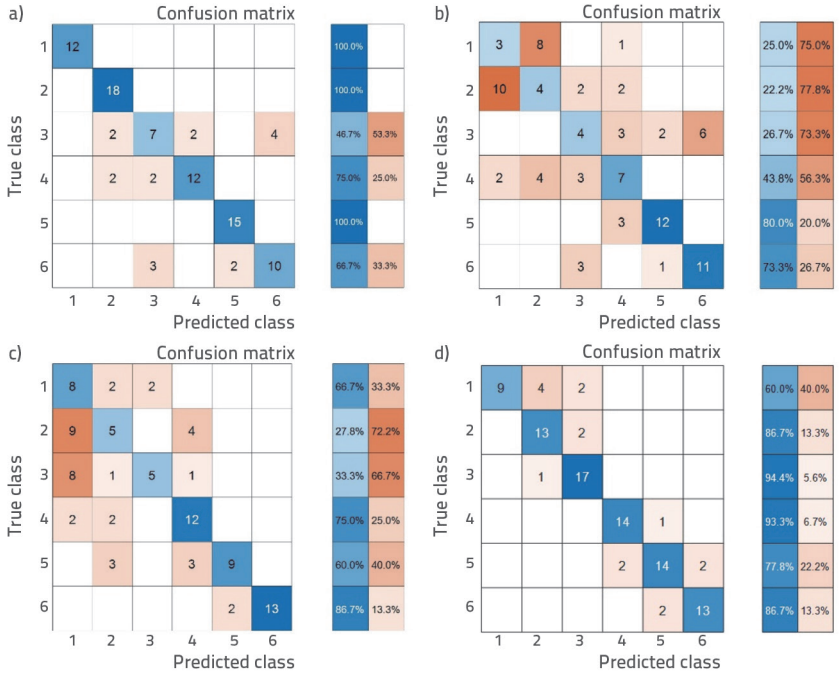

Figure 13. Confusion matrix of vehicle weight classification at 30 km/h: a) short-term energy; b) spectral centroid; c) spectral entropy; d) energy entropy

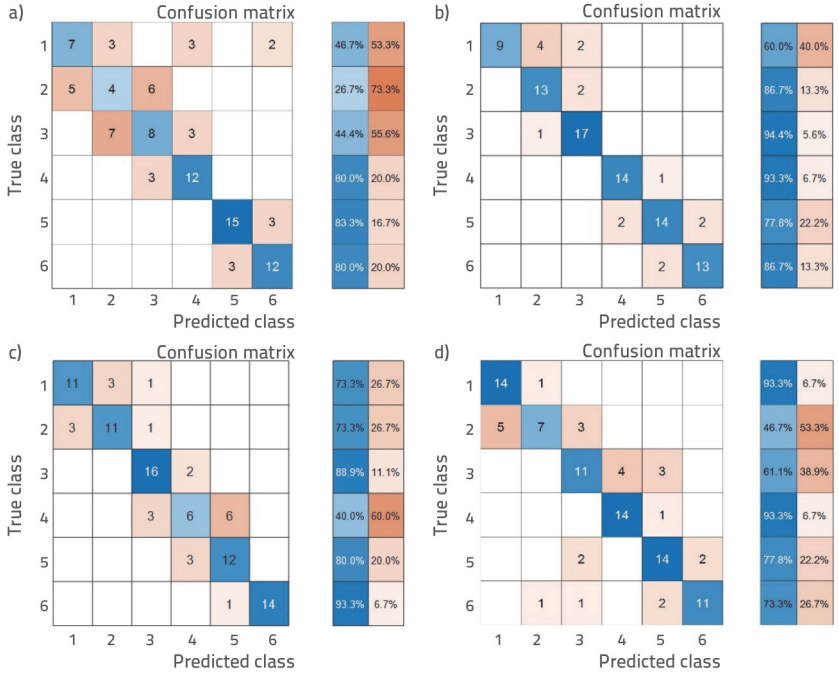

Figure 14. Confusion matrix of vehicle weight classification at 50 km/h: a) short-term energy; b) spectral centroid; c) spectral entropy; d) energy entropy

As shown in Figure 13, at a lower speed of 30 km/h, the use of short-term energy and energy entropy features for identifying vehicle weight yielded better performance than that of using the spectral centroid and spectral entropy. Among these, energy entropy exhibited the highest performance, achieving a complete accuracy of 90.8 %. The confusion matrix indicates that even when misclassification occurs, the errors are typically confined to the adjacent level, suggesting a certain recognition capability. Short-term energy performance performed second best, with approximately 10 % probability of misclassifying into nonadjacent load levels. However, the recognition accuracy based on the spectral centroid and entropy was substantially low, and the confusion matrix showed suboptimal regularity.

Figure 14 illustrates that at higher speeds of 50 km/h, the recognition effect based on the spectral centroid and spectral entropy improved compared to that based on short-term energy and energy entropy. Among these, the spectral centroid performed the best, achieving a complete accuracy of 83.1 %. The confusion matrix indicates that even in instances of misclassification, the data points are predominantly classified to the adjacent level, indicating a certain recognition capability. This is consistent with the conclusions of the analysis presented in sections 4.3 and 4.4. The recognition accuracy based on energy entropy is relatively low, and the confusion matrix indicates an approximately 10 % probability of identifying nonadjacent load levels. The complete accuracy of recognition based on short-term energy is also low. However, when considering the classification of adjacent levels, its

performance was comparable to that based on energy entropy.

As shown in Figures 13 and 14, most misclassifications were close to the correct categories in the confusion matrix for vehicle weight classification based on EMD energy entropy. In addition, at high vehicle speeds, the recognition results based on the spectral centroid and spectral entropy were symmetrical along the diagonal of the confusion matrix, indicating good recognition accuracy. In future research, it is likely beneficial to explore the fusion of two or more features and the application of advanced recognition algorithms, particularly under conditions involving large samples, to further enhance classification performance.

6. Conclusion

The acoustic signal components of vehicle tripping at expansion joints are complex, and the signal characteristics associated with vehicle weight are unknown; therefore, the contradiction between calculation efficiency and spectrum leakage must be comprehensively incorporated in the interception and pre-processing of acoustic signals. The analysis results in this study suggest that the sampling frequency must not be extremely low, and the threshold method based on the trend line of the sound pressure amplitude must be used to detect and intercept the acoustic signal of the impact, which can effectively retain the effective signal related to the vehicle weight.

The correlation analysis results between various acoustic signal features and vehicle weight indicate a significant correlation between short-term energy, spectral centroid, spectral entropy, EMD energy entropy, and vehicle weight. With small samples, the KNN classifier was used to identify the vehicle weight based on the above four acoustic signal characteristics, and the comprehensive and accurate recognition rate and confusion matrix result judgment were effective.

The results of vehicle weight recognition based on the KNN classifier indicate that the overall recognition performance follows the order: EMD energy entropy>spectral entropy/ spectral centroid> short-term energy. However, performance of different feature recognition methods varies with vehicle speed, indicating that vehicle weight recognition must incorporate the impact of vehicle speed. This study demonstrated that the vehicle weight recognition method based on the tripping acoustic signal at the expansion joint can further increase the number of samples and feature fusion, potentially resulting in higher-precision vehicle weight recognition.

Acknowledgments

The research described in This study was financially supported by the National Natural Science Foundation of China (51678253), Natural Science Foundation of Hunan Province (2020JJ5195), and the Scientific Research Foundation of Hunan Provincial Education Department (CN) (20B218). We gratefully acknowledge this support.

REFERENCES

[1] Jacob, B., van Loo, H.: Weigh-in-motion for enforcement in Europe, Proceedings of The International Conference on Heavy Vehicles, HV Paris, 2013., pp. 25-38

[2] Ministry of Transport of China: 2020 Statistical Bulletin on the Development of the Transportation Industry, China Transport News, 2021.

[3] Hou, R., Jeong, S., Lynch, J.P., et al.: Law, data-driven analytical load rating method of bridges using integrated bridge structural response and weigh-in-motion truck data, Mech. Syst. Sig. Process., 163 (2022) 4, Paper 108128, https://doi.org/10.1016/j.ymssp.2021.108128

[4] Ren, W.X., Zuo, X.H., Wang, N.B., et al.: Review of non-pavement bridge weigh-in-motion, China J. Highw. Transp., 27 (2014) 7, pp. 45-53

[5] Longwei, Z., Jianqun, W. et al.: Theoretical and experimental study on a bridge weigh-in-motion iterative algorithm, J. Vib. Shock, 40 (2021) 6, pp. 171-176

[6] Chen, S.Z., Wu, G., Feng, D.C.: Development of a bridge weigh-in-motion method considering the presence of multiple vehicles, Eng. Struct., 191 (2019), pp. 724–739

[7] Kawakatsu, T., Aihara, K., Takasu, A., et al.: Deep sensing approach to single-sensor vehicle weighing system on bridges, IEEE Sens. J., 19 (2018) 1, pp. 243–256

[8] Lu, D., Xin, L., Yang, L.T., et al.: Bridge weigh-in-motion algorithm considering multi-vehicle based on convolutional neural network, J. Hunan Univ. Nat. Sci., 49 (2022) 1, pp. 33-41

[9] Xuan, K., Jie, Z., Teng-yi, W., et al.: Non-contact vehicle weighing method based on tire deformation using image recognition, China J. Highw. Transp., 35 (2022) 8, pp. 186-193

[10] Feng, M.Q., Leung, R.Y.: Application of computer vision for estimation of moving vehicle weight, IEEE Sens. J., 21 (2020) 10, pp. 11588-11597

[11] McKay, T.R., Salvaggio, C., Faulring, J.W., et al.: Remotely detected vehicle mass from engine torque-induced frame twisting, Opt. Eng., 56 (2017) 6, pp. 063101

[12] Ojio, T., Carey, C., Obrien, E.J., et al.: Contactless bridge weigh-in-motion, J. Bridge Eng., 21 (2016) 2, pp. 1084-0702

[13] Xialin, M.A., Ming, M.C., Jianli, D.: Audio identification of vehicle type based on frequency analysis and support vector machine, J. Appl. Acoust., 33 (2014) 4, pp. 371-376

[14] George, J., Mary, L., Riyas, K.S.: Vehicle detection and classification from acoustic signal using ANN and KNN, Proceedings of The International Conference on Control Communication and Computing (ICCC), 2013., pp. 436-439

[15] Xiaoxuan, Q., Li, D., Guoshan, Z.: Vehicle type recognition by acoustic signal based on wavelet packet decomposition and approximate entropy, J. Nanjing Univ. Sci. Technol., 44 (2020) 1, pp. 67-79

[16] Frederick, H., Winda, A., Solihin, M.I.: Automatic petrol and diesel engine sound identification based on machine learning approaches, E3S Web of Conferences, 130 (2019), pp. 130:01011

[17] Hongxu, Z., Yiwen, Z., Wenshuai, Y.: Research on model identification of hybrid vehicle audio signal based on support vector machine, Laser J., 39 (2018) 9, pp. 133-137

[18] Guo, B., Nixon, M.S., Damarla, T.: Improving acoustic vehicle classification by information fusion, Pattern Anal. Applic., 15 (2012) 29, pp. 29-43

[19] Jiamei, Z., Wencheng, H.U., Congshuang, J, et al.: The vehicle type and speed recognition based on acoustic signal characteristics, J. Appl. Acoust., 40 (2021) 3, pp. 468-473

[20] Chen, H., Zhang, Z.: Hybrid neural network based on novel audio feature for vehicle type identification, Sci. Rep., 11 (2021) 1, pp. 1-10

[21] ISO 10844:2014: Specification of test tracks for measuring noise emitted by road vehicles and their tyres, 2014.

[22] Yong, X.: Characteristics and spectrum evaluation of outside noise on asphalt pavements as vehicle-tire-road coupling, Southeast University, Nanjing, 2017.

[23] Algohi, B., Mufti, A., Thomson, D.: Detection of speed and axle configuration of moving vehicles using acoustic emission, J. Civ. Struct. Health Monit., 8 (2018) 3, pp. 353-362

[24] Wieczorkowska, A., Kubera, E., Słowik, T., et al.: Spectral features for audio-based vehicle and engine classification, J. Intell. Inf. Syst., 50 (2018) 2, pp. 265-290

[25] Ravshanovich, K.A., Yamaguchi, H., Matsumoto, Y., et al.: Mechanism of noise generation from a modular expansion joint under vehicle passage, Eng. Struct., 29 (2007) 9, pp. 2206-2218

[26] Ghimire, J.P., Matsumoto, Y., Yamaguchi, H.: Numerical investigation of noise generation and radiation from an existing modular expansion joint between prestressed concrete bridges, J. Sound Vib., 328 (2009) 27, pp. 129-147

[27] Yang, Y., Junping, L., Linze, S., et al.: Field-measurement research on the noise at bridge expansion joints under vehicular load, Shanghai Environmental Sciences, 36 (2017) 6, pp. 9-13

[28] Guo, B., Nixon, M.S., Damarla, T.: Improving acoustic vehicle classification by information fusion, Pattern Anal. Applic., 15 (2012) 29, p. 43

[29] Yu, Y., Junsheng, C.: A roller bearing fault diagnosis method based on EMD energy entropy and ANN, J. Sound Vib., 294 (2006)1-2, pp. 269-277

[30] Fei, S., Chao, C., Jiawen, X., et al.: Application of spectral centroid transfer in bearing fault diagnosis under varying working conditions, Chinese Journal of Scientific Instrument, 40 (2019) 5, pp. 99-108

[31] Sharma, G., Umapathy, K., Krishnan, S.: Trends in audio signal feature extraction methods, Appl. Acoust., 2020.

[32] Qingqi, L.U., Yanyan, B.: A speech endpoint detection algorithm based on dual-threshold two sentences, Electron. Sci. Tech., 25 (2012) 1, pp.13-19

[33] Hou, Y., Zhou, C., Changming Tian, et al.: Acoustic feature enhancement in rolling bearing fault diagnosis using sparsity-oriented multipoint optimal minimum entropy deconvolution adjusted method, Appl. Acoust., 2022, pp. 201

[34] Li, X., Wan, S., Liu, S., Zhang, Y., Hong, J., et al.: Bearing fault diagnosis method based on attention mechanism and multilayer fusion network, ISA Trans., 128 (2022), pp. 550-564

[35] Di, P., Jianhai, Y., Jing, J.: Weak fault feature extraction of rolling bearing based on autocorrelation and energy operator enhancement, J. Vib. Shock, 40 (2021) 11, pp. 101-123

[36] Shi, H., Li, Y., Bai, X., et al.: A two-stage sound-vibration signal fusion method for weak fault detection in rolling bearing systems, Mech. Syst. Signal Process., 172 (2022), p. 109012

[37] Yang, D., Lv, Y., Yuan, R., Yang, K., et al.: A novel vibro-acoustic fault diagnosis method of rolling bearings via entropy-weighted nuisance attribute projection and orthogonal locality preserving projections under various operating conditions, Appl. Acoust., 196 (2022), p. 108889

[38] Mian, T., Choudhary, A., Fatima, S.: An efficient diagnosis approach for bearing faults using sound quality metrics, Appl. Acoust., 195 (2022), p. 108839

[39] Wang, Y.S., Liu, N.N., Guo, H., et al.: An engine-fault-diagnosis system based on sound intensity analysis and wavelet packet pre-processing neural network, Eng. Appl. Artif. Intell., 194 (2020), p.103765

[40] Chen, L., Wang, C., Chen, J., et al.: Voice disorder identification by using Hilbert-Huang transform (HHT) and K nearest neighbor (KNN), J. Voice, 35 (2021) 6, p. 932.e1-932.e11

[41] Xiang, L., Yan, W., Baoqing, L.: Acoustic signal classification of field vehicles based on combination of LSTM and CNN, Piezoelectrics and acoustooptics, 43 (2021) 3, pp. 379-384

[42] Khoshouei, M., Bagherpour, R.: Predicting the geomechanical properties of hard rocks using analysis of the Acoustic and vibration signals during the drilling operation, Geotech. Geol. Eng., 39 (2021), pp. 2087-2099

[43] Hamid, O.K.: Frame blocking and windowing speech signal, J. Inf. Commun. Intell. Syst., 4 (2018), pp. 87–94

[44] Szwajcowski, A., Pilch, A.: Optimization of piano tuning by means of spectral entropy minimization, Appl. Acoust., 166 (2020), p. 107359

[45] Pan, C., Huang, Z., You, J., et al.: Moving force identification based on sparse regularization combined with moving average constraint, J. Sound Vib., 515 (2021), p. 116496

[46] Laxman, K.C., Ross, A., Ai, L., et al.: Determination of vehicle loads on bridges by acoustic emission and an improved ensemble artificial neural network (KNN), Constr. Build. Mater., 364 (2023), p. 129844

[47] Li, Y., Tang, B., Geng, B., Jiao, S.: Fractional order fuzzy dispersion entropy and its application in bearing fault diagnosis, Fractal Fract. 6 (2022), p. 544

[48] Li, Y., Geng, B., Tang, B.: Simplified coded dispersion entropy: A nonlinear metric for signal analysis, Nonlinear Dyn., 111 (2023), pp. 9327-9344